DOI: 10.1002/ejic.200900496

A Dinuclear Double-Stranded Oxido Complex of Re^V with a Bis(benzene-*o*-dithiolato) Ligand

Jorge S. Gancheff,[a] Rodrigo Q. Albuquerque,[b] Andrés Guerrero-Martínez,[b] Tania Pape,[a] Luisa De Cola,[b] and F. Ekkehardt Hahn*[a]

Keywords: Oxido complexes / Rhenium(V) / Double-stranded complexes

The reaction of $[ReOCl_3(PPh_3)_2]$ with 1,2-bis(2,3-dimercaptobenzamido)ethane (H_4-**1**) in the presence of Na_2CO_3 in methanol under anaerobic conditions affords the dinuclear Re^V oxido complex $[PPh_4]_2[ReO(\mathbf{1})]_2$ containing two distorted square-pyramidal $\{Re^VOS_4\}$ units bridged by the ligand strands in a double-stranded fashion. The coordination geometry around the metal centers is similar to the one observed for $[ReO(bdt)_2]^-$. The ReS_4 planes are arranged in a coplanar fashion and are not twisted around the metal–metal vector, which prevents the complex to adopt a helical structure. Luminescence studies show the presence of emission bands, which are assigned to singlet-singlet transitions exhibiting very fast decays (ca. 10 ns). Theoretical Density Functional (DFT) studies on geometry and electronic properties were performed employing the hybrid B3LYP and PBE1PBE functionals. While the general trends observed in the experimental data are well reproduced in all cases, a good agreement was obtained using PBE1PBE, in particular for the Re–S bonds. Natural Bond Orbitals (NBO) analysis indicates the presence of polarized Re≡O and Re–S bonds, both of them polarized toward the non-metal. The calculation show that the molecular orbitals of the Re^V are doubly degenerated, the occupied 5d orbital of rhenium lying beneath occupied sulfur-based MOs due to the rigid geometry imposed by the C–C backbone of the bis(benzene-*o*-dithiolato) ligands. The origin of all absorption bands is ascribed to a ligand-to-metal charge transfer (LMCT), in which occupied sulfur-based orbitals and unoccupied rhenium-centered orbitals are involved.

Introduction

Oxido complexes of Re^V have received considerable attention in the past few years. Particular interests have been aroused due to their reactivity, their photochemical and spectroscopic properties and their role in catalytic processes and oxygen atom transfer (OAT) reactions.[1–9] Furthermore, due to the nuclear decay of ^{186}Re, rhenium complexes found very promising radiopharmaceutical applications.[10–13] Rhenium oxido complexes containing dithiolato ligands in particular, have been studied with different purposes. For example, mechanistic aspect of OAT reactions have been studied with complexes of type $[ReO(CH_3)(SCH_2C_6H_4S)X]$ (X = substituted pyridine or alkyl and aryl phosphanes) by Lathi and Espenson,[14] and a comprehensive DFT study on these systems has been carried out Yang and Hall.[15] Noll[16] et al. have synthesized neutral complexes of type [ReO(SNSS)] [SNSS = S–CH_2CH_2–S–CH_2CONH–CH(COOR)CH_2S] for radiopharmaceutical applications. The affinity of oxido complexes of Re^V with quinolyl moieties as anchor groups for serotonin receptors has been studied by A. Zablotskaya et al.[17]

Bis(benzene-*o*-dithiolato) (hereafter referred to as bis-bdt) ligands containing two benzene-*o*-dithiolato (bdt) donor groups have been known since 1995 when a first synthetic protocol leading to such ligands was reported.[18] The synthesis of such ligands was later studied in detail.[19] Bis-bdt ligands were later used to construct helical supramolecular assemblies.[20] This type of ligand does not only allow the generation of novel complex architectures, but metal complexes with bdt ligands also exhibit remarkable electronic and structural properties.[19–23] Over the past years bis-bdt complexes of titanium(IV),[21–23] iron(III),[22,23] cobalt(III),[20,21c–21d,23] nickel(II),[21c–21d,23] and nickel(III)[21c–21d,23] were synthesized and their properties studied. The studies of the coordination chemistry of bis-bdt ligands have focused on first-row transition metals, while complexes with heavier transition metals remained largely unknown.

Herein, we describe the synthesis and the photophysical properties of novel dinuclear complex of Re^V containing a bis-bdt ligand, in which ethylenediamide acts as a bridge

[a] Institut für Anorganische und Analytische Chemie der Westfälischen Wilhelms-Universität Münster,
Corrensstrasse 30, 48149 Münster, Germany
Fax: +49-251-833-3108
E-mail: fehahn@uni-muenster.de
[b] Physikalisches Institut, Westfälische Wilhelms-Universität Münster,
Mendelstrasse 7, 48149 Münster, Germany

Supporting information for this article is available on the WWW under http://dx.doi.org/10.1002/ejic.200900496.

connecting the bdt units and the metal component is present as oxido metal ion ReO^{3+}. The bis-bdt ligand has been described previously and is known to form either double- or triple-stranded dinuclear complexes with first-row transition metal ions.[20] To gain insight into the bonding situation existing in the dinuclear Re^{V} complexes with two bis-bdt ligands, theoretical studies on the equilibrium geometry and the electronic properties by means of Density Functional Theory (DFT) methods were also carried out. To the best of our knowledge we do not know of any DFT studies on this type of dinuclear complexes. The computational results presented here constitute an entry into the assessment of the electronic and structural properties of dinuclear complexes containing bis-bdt ligands.

Results and Discussion

Synthesis and Crystal Structure

Usually, complexes with bis-bdt ligands are prepared by a metathesis reaction of highly reactive alkali metal bis(benzene-*o*-dithiolates) with metal halide under salt elimination. The use of alkali bis(benzene-*o*-dithiolates) as well as ligand transfer reactions have been employed successfully to obtain dinuclear double-stranded complexes with bis-bdt ligands.[20,21c,23] We have reacted 1,2-bis(2,3-dimercaptobenzamido)ethane H_4-**1** with the Re^{V} precursor $[ReOCl_3(PPh_3)_2]$ containing the oxido metal ion ReO^{3+} in the presence of Na_2CO_3 as a base. This method has previously been employed for the generation of mononuclear thiolato complexes with the ReO^{3+} cation.[24–27] For example, Clegg[28] has prepared $(PPh_4)[ReO(bdt)_2]$ starting from H_2bdt and $[ReOCl_3(PPh_3)_2]$ in methanol in the presence of Et_3N and PPh_4Br as source of large counterions. In analogy, ligand H_4-**1** reacts in the molar ratio 1:1 with $[ReOCl_3(PPh_3)_2]$ in the presence of Na_2CO_3 to give the salt $(PPh_4)_2[ReO(\mathbf{1})]_2$ after addition of PPh_4Cl (Scheme 1). The formation of the compound was indicated by a a peak at m/z = 595 with the correct isotope distribution for the dianion $[ReO(\mathbf{1})]_2^{2-}$ in the ESI MS (negative ions) mass spectrum.

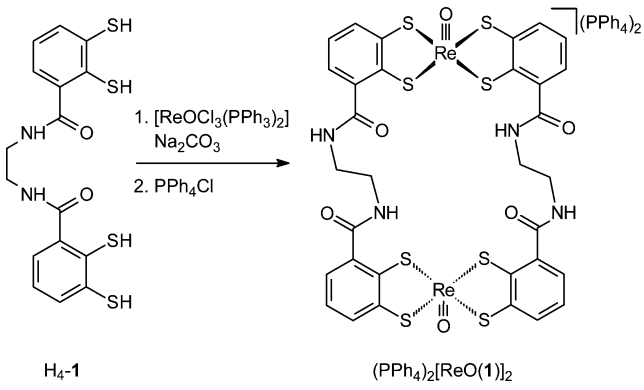

Scheme 1. Synthesis of complex $(PPh_4)_2[ReO(\mathbf{1})]_2$.

Orange, air-stable crystals of $(PPh_4)_2[ReO(\mathbf{1})]_2 \cdot 2DMF$ were obtained from a saturated DMF solution of $(PPh_4)_2[ReO(\mathbf{1})]_2$ at ambient temperature. The X-ray diffraction structure analysis (Figure 1) shows the complex anion residing on a crystallographic inversion center. The complex anion contains two distorted square-pyramidal $\{Re^{V}OS_4\}$ (τ = 0.593)[29] units bridged in a double-stranded fashion. The Re–O vectors are oriented in *anti*-orientation. The coordination environment around the rhenium atoms resembles the geometry found in the anion $[ReO(bdt)_2]^-$.[28,30] The rhenium atom is situated 0.73 Å above the plane of the four sulfur atoms while the C_6S_2 donor groups are essentially planar. A Re–O bond length [Re–O3 1.705(7) Å] typical for complexes of the ReO^{3+} oxido ion have been found in $[ReO(\mathbf{1})]_2^{2-}$, indicating the presence of a Re≡O triple bond.[31]

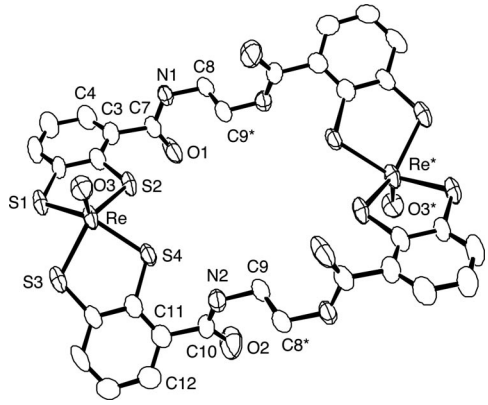

Figure 1. Molecular structure of the $[ReO(\mathbf{1})]_2^{2-}$ anion in $(PPh_4)_2[ReO(\mathbf{1})]_2 \cdot 2DMF$ with the crystallographic numbering scheme. Hydrogen atoms, counterions and solvent molecules have been omitted for clarity. The anion resides on a crystallographic inversion center. Selected bond lengths [Å] and angles [°]: Re–S1 2.317(3), Re–S2 2.309(3), Re–S3 2.313(3), Re–S4 2.318(3), Re–O3 1.705(7); S1–Re–S2 84.69(10), S1–Re–S3 82.86(11), S1–Re–S4 147.00(10), S1–Re–O3 106.2(3), S2–Re–S3 137.26(10), S2–Re–S4 84.05(11), S2–Re–O3 111.3(3), S3–Re–S4 86.64(11), S3–Re–O3 114.4(3), S4–Re–O3 106.8(3).

In principle, dinuclear complex with bis-bdt ligands featuring two planar $\{M(bdt)_2\}$ coordination polyhedra, can form helical structures.[21c] For such helicity in a dinuclear complex, it would be necessary that the plane containing the $M(bdt)_2$ planes are arranged in a non-coplanar fashion and thus are twisted around the metal–metal vector. This type of helicity was not found in the anion $[ReO(\mathbf{1})]_2^{2-}$, where the $\{ReO(bdt)_2\}$ coordination polyhedra are arranged in a coplanar fashion. To the best of our knowledge, complex anion $[ReO(\mathbf{1})]_2^{2-}$ constitutes the first example for a dinuclear complex containing two independent $\{ReO(bdt)_2\}$ units bridged in a double-stranded fashion.

Spectroscopic Measurements

Compound $(PPh_4)_2[ReO(1)]_2$ was further characterized by means of absorption and luminescence (emission and excitation) spectroscopy. The absorption spectrum recorded

at ambient temperature in DMF is shown in Figure 2. The assignment of the absorptions is discussed in detail in the section *Electronic Spectra*.

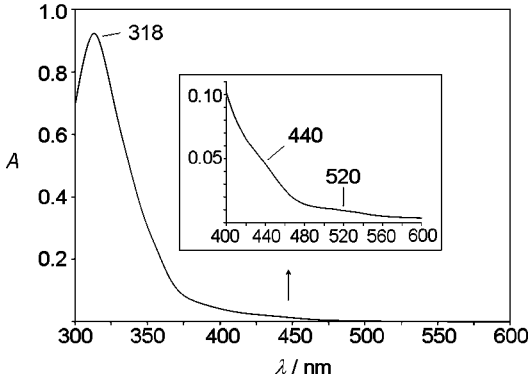

Figure 2. UV/Vis absorption spectrum of $(PPh_4)_2[ReO(1)]_2$ in DMF.

The emission spectrum of the Re^V complex, together with its excitation spectrum, both at ambient temperature in DMF are shown in Figure 3. Upon excitation at 290 nm, with population of the ligand-centered (LC) state, a weak luminescence can be observed. However, excitation of the complex at 370 nm, where one ligand-to-metal charge transfer (LMCT) band is located, produces a much stronger luminescence. This is nicely seen from the excitation spectrum, which was recorded by monitoring the emission at λ = 480 nm (Figure 3, dashed line). The emission spectrum, recorded with excitation at λ = 325 nm, exhibits a peak at ca. 410 nm, as shown in Figure 3 (solid line). The blue emission of the Re^V complex shows a fast decay [t = 10 ns, λ(excitation) = 402 nm, λ(detection) = 450 nm]. This blue emitting complex is strongly quenched upon increasing of the concentration, which suggests that aggregation takes place. Indeed, π-π stacking can be observed the crystallographic unit cell of $(PPh_4)_2[ReO(1)]_2$, suggesting that such interactions may also occur in solution at higher concentrations.

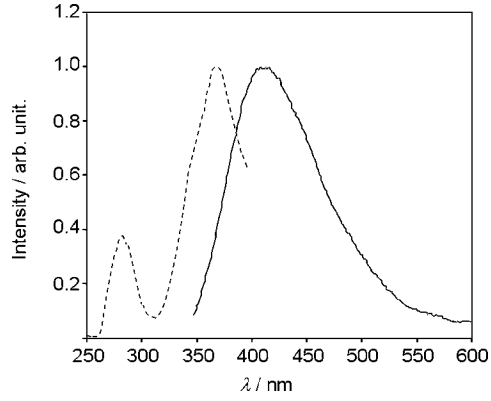

Figure 3. Emission spectrum [solid line, λ(excitation) = 325 nm] and excitation spectrum (dashed line), λ(emission = 480 nm) of $(PPh_4)_2[ReO(1)]_2$ in DMF at ambient temperature.

Geometry Optimization, Electronic Structure and NBO Analysis

The use of PBE1PBE in combination with STMIDI (see section *Computational Details*) has been used to describe the Re–S bonds, not only in mononuclear complexes but also in large transition metal complexes with thiolato ligands.[32] This method has proved to adequately describe Re–S bonds with very low computational cost.[32] We therefore used four DFT methodologies to study structural and electronic properties of $(PPh_4)_2[ReO(1)]_2$, namely, B3LYP and PBE1PBE in combination with LANL2DZ and STMIDI. These DFT methods will hereafter be called BLDZ (B3LYP and LANL2DZ), BSTM (B3LYP and STMIDI), PLDZ (PBE1PBE and LANL2DZ) and PSTM (PBE1PBE and STMIDI), respectively.

The optimizations starting from the crystallographically determined molecular structure lead to a minimum as stationary point. Selected optimized parameters are presented in Table 1. The general trends observed in the crystallographical data are well reproduced in the calculations. Calculated bond lengths and angles are in good agreement with the values obtained from the X-ray diffraction study. The presence of the terminal oxido ligand results in the metal center residing 0.7 Å out the plane defined by the four sulfur donor atoms, while the atoms in the C_6S_2 donor groups form one plane.

Table 1. Selected bond parameters calculated for $[ReO(\mathbf{1})]_2^{2-}$ in a closed-shell d^2 configuration (singlet) by using the BLDZ, BSTM, PLDZ and PSTM methods (T = 298 K).[a]

Method	Bond	d [Å]	Angle	∠ [°]
BLDZ	Re–O3	1.706	O3–Re–S1	108.5
	Re–S1	2.415	O3–Re–S2	108.3
	Re–S2	2.401	S1–Re–S2	84.4
	Re–S3	2.415	S1–Re–S3	83.5
	Re–S4	2.401		
BSTM	Re–O3	1.687	O3–Re–S1	108.6
	Re–S1	2.336	O3–Re–S2	109.2
	Re–S2	2.330	S1–Re–S2	84.4
	Re–S3	2.336	S1–Re–S3	83.0
	Re–S4	2.330		
PLDZ	Re–O3	1.695	O3–Re–S1	108.5
	Re–S1	2.386	O3–Re–S2	108.3
	Re–S2	2.375	S1–Re–S2	84.7
	Re–S3	2.386	S1–Re–S3	83.2
	Re–S4	2.375		
PSTM	Re–O3	1.676	O3–Re–S1	108.7
	Re–S1	2.312	O3–Re–S2	109.4
	Re–S2	2.306	S1–Re–S2	84.6
	Re–S3	2.312	S1–Re–S3	82.6
	Re–S4	2.306		

[a] For atom assignment see Figure 1.

The calculated Re–S bond lengths range from 2.306 to 2.415 Å (experimental average value 2.314 Å). The Re–S bond lengths are the most sensitive parameters in the DFT methods employed. The use of the STMIDI basis set leads to a remarkable improvement of the calculated Re–S lengths in comparison with the LANL2DZ method. When the STMIDI basis set is combined with PBE1PBE, the value closest to the experimental value is obtained for the

Re–S bond length. These results are in line with the data previously reported for $[ReO(bdt)_2]^-$.[32]

The calculated Re–O bond lengths range from 1.676 to 1.706 Å [experimental value 1.705(7) Å]. These calculated lengths, in all cases, fall into the range experimentally determined for Re≡O triple bonds (1.691 ± 0.05 Å).[31] The best calculated results were obtained with the BLDZ method with a residual deviation of 0.001 Å. All the other methodologies underestimate this bond length. In contrast with the results obtained for the Re–S bonds, PSTM does not give the best description of the Re–O bond. These results are in agreement with the performance of the aforementioned method in describing Re–O bond reported in $[ReO(bdt)_2]^-$.[32]

In spite of starting from the X-ray diffraction data (Figure 1), the optimized geometry shows a different conformation of the spacer (Figure 4). This effect could possibly be induced by a different orientation of the carbonyl groups. The calculations lead to an almost coplanar arrangement of the planes O1–C7–C3 and C7–C3–C4 (Figure 1) which was not observed in the molecular structure determination (for atom assignment see Figure 1). In contrast to the crystallographic dihedral angles of 98.8° and 60.9° for the O1–C7–C3–C4 and O2–C10–C11–C12, respectively, the calculated value is 19.3° (with all DFT methods), leading to a stair-type optimized structure (Figure 4).

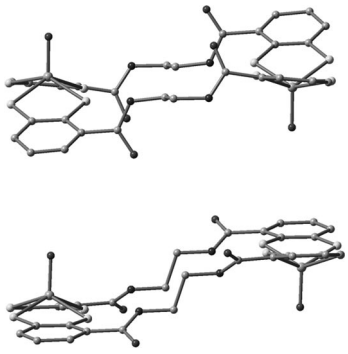

Figure 4. Comparison between the crystallographic (top) and calculated (bottom) structures of the $[ReO(1)]_2^{2-}$ anion.

Table 2 contains the results of the Natural Population Analysis (NPA). The calculated charges on rhenium are considerable lower than the formal charge of +5 as a product of a significant electron donation from the oxido and the thiolato ligands. With the BLDZ method the monooxido core carries a charge of +0.18, while the PSTM method leads to a charge of +0.02. These results are in line with the data reported for $[ReO(bdt)_2]^-$.[32]

Due to the symmetry of the optimized structure at all levels of DFT theory, all natural orbitals involving rhenium have the same character in both monooxido units. Therefore, only the analysis of one of them is presented and discussed. In Table 3 the bond nature analysis for $[ReO(\mathbf{1})]_2^{2-}$ as obtained using BLDZ is shown (the results obtained with the other methods are included in the Supporting Information, Tables S1–S3).

Table 2. Atomic charges from the NPA analysis for $[ReO(\mathbf{1})]_2^{2-}$ in a closed shell d^2 configuration (singlet) by using BLDZ, BSTM, PLDZ and PSTM DFT methods (T = 298 K).[a]

Method	Re	S1	S2	O3
BLDZ	0.648	–0.119	–0.075	–0.470
BSTM	0.544	0.000	–0.009	–0.465
PLDZ	0.606	–0.064	–0.111	–0.461
PSTM	0.493	–0.024	0.016	–0.468

[a] For atom assignment see Figure 1.

Table 3. Population and contribution (%) of atomic orbitals to selected natural bond orbitals (NBO) between rhenium, the sulfur atoms and the oxido ligand of $[ReO(\mathbf{1})]_2^{2-}$, employing the BLDZ method.[a]

Bond	Population[b]	% Re	% X	% ns	% np	% (n–1) d
Re–O(1)	1.98 (0.26)	28.54		12.40	0.82	86.78
			71.46	20.11	79.89	
Re–O(2)	1.82 (0.33)	20.99			29.92	70.08
			79.01		100.0	
Re–O(3)	1.81 (0.31)	20.89		0.02	31.83	68.15
			79.11		100.0	
Re–S1	1.77 (0.25)	22.71		20.87	35.04	44.09
			77.29	14.20	85.80	
Re–S2	1.78 (0.27)	21.57		21.86	33.17	44.97
			78.43	14.41	85.59	
Re–S3	1.77 (0.25)	22.70		20.91	35.02	44.08
			77.30	14.20	85.80	
Re–S4	1.78 (0.27)	21.51		21.90	33.14	44.97
			78.49	14.46	85.54	

[a] For atom assignment see Figure 1. X represents the non-metallic atoms (O and S); n = 6 for Re, n = 3 for S, n = 2 for O. Population represents the population of the Re–O or Re–S bonds. % Re gives the contribution of the bond at rhenium; % X gives the contribution of the bond at the non-metal atom; % ns, % np and % (n–1)d give the hybridization of the bond. For each bond, in the first and second rows the hybridization at the metal and non-metal respectively are given. [b] The first value gives the population of the bond; the population of the corresponding *anti* bond in parentheses.

Three natural Re–O bonds were detected, consisting of bonding contributions by one σ and two π bonds. The Re–O σ bond is strongly polarized towards the oxygen atom. The metal contribution to this bond is 28.54%. The Re–O π bonds are even more polarized and the metal contribution amounts to about 21%. The *s* and particularly the *p* contributions characterize the Re–O bond as a donor-acceptor bond. The hybridization at rhenium shows clearly that the *d* contribution dominates the Re–O σ and π bonds. This description of the Re–O bonds is in agreement with the results of a few studies regarding the analysis of the bonding situation in transition metal oxido complexes.[32–36]

All sulfur donor atoms participate in σ bonds. The hybridization at the metal atom shows mainly *d* character and at the non-metal exhibits mainly *p* character. A strong polarization toward the non-metal was detected, the contribution of rhenium being about 22%. These results are in agreement with parameters discussed for the Re–O bond in $[ReO(bdt)_2]^-$.[32]

Molecular Orbital Description

Figure 5 shows a partial molecular orbital energy diagram derived from the BLDZ calculations.

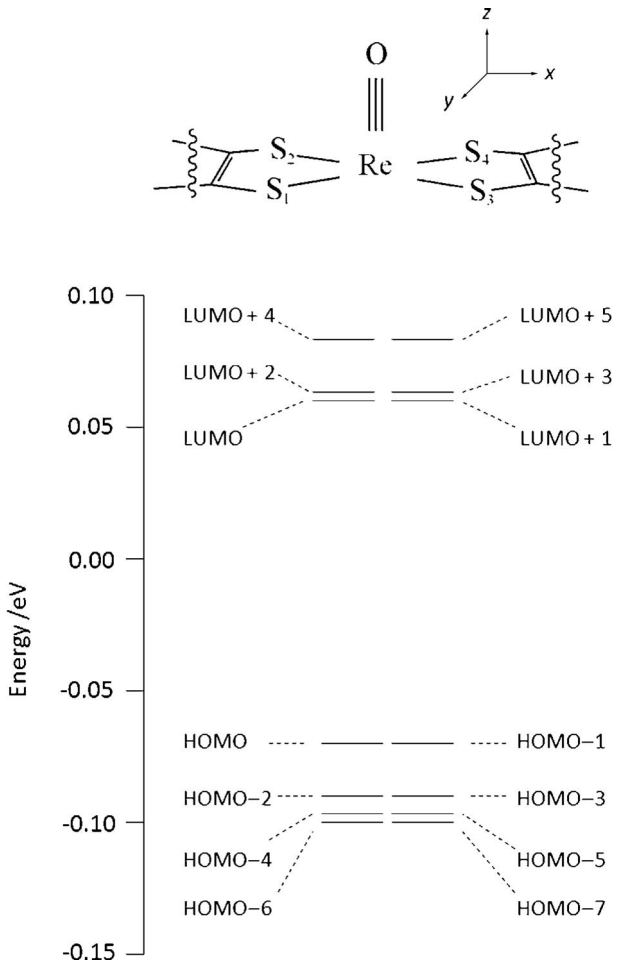

Figure 5. Molecular orbital energy diagram for eight occupied and six unoccupied MOs of $[ReO(1)]_2^{2-}$ as obtained from the BLDZ DFT methodology.

The analysis of MOs is relevant to gain insight into the chemical bonding between the metal atom and the thiolato ligands and for the further understanding of the optical properties. It has been reported that calculated transition energies correlate strongly with the DFT functional.[37–39] The BLDZ method has been shown to be sufficient for the calculation of spectral properties of rhenium complexes.[33,40] Therefore results obtained with the BLDZ methodology are presented and discussed and those obtained with the other methods are included in the Supporting Information (see Tables S4–S9 for further details of values of oscillator strengths, and origin of electronic transitions).

The symmetry of the optimized geometry gives rise to an energy diagram, in which all MOs show double degeneracy. The strong σ and π donor properties of the oxido ligand destabilize the $5d_{z^2}$ and the $5d_{xz/yz}$ orbitals within the *d* orbital manifold. The calculation is able to reproduce the rhenium *d* orbital manifold resulting from the presence of a terminal oxido ligand.[41,42] The electronic configuration for rhenium in $[ReO(1)]_2^{2-}$ is formally $5d^2$. These electrons reside in a MO with an important contribution of the $d_{x^2-y^2}$ orbital, to give a singlet ground state. The filled rhenium-based orbitals for both monooxido units in $[ReO(1)]_2^{2-}$ (HOMO–4 and HOMO–5) (Figure 6) lie below the benzodithiolato-based π orbitals which define the highest occu-

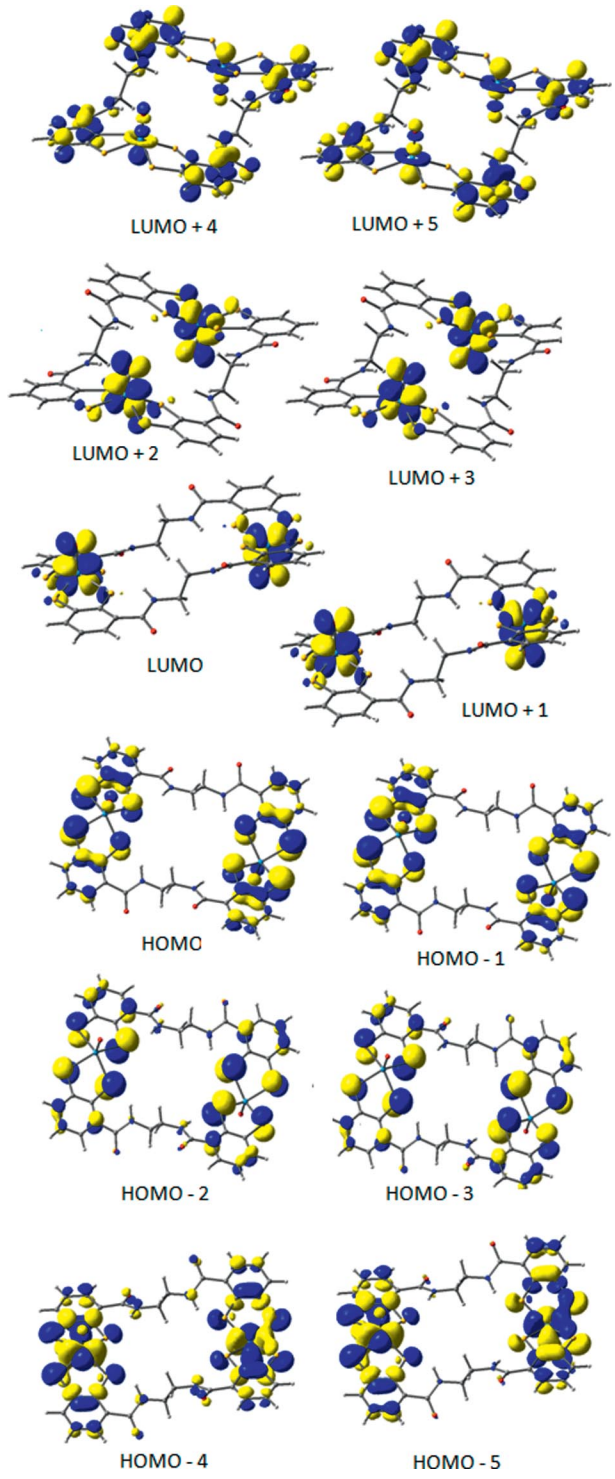

Figure 6. Contour of selected MOs of $[ReO(1)]_2^{2-}$ as obtained from the BLDZ methodology.

pied orbitals (HOMO and HOMO–1). Beneath the occupied MOs of rhenium, there are a set of sulfur-based orbitals, for which the in-plane orbitals are in general more energetically stabilized with respect to out-of-plane orbitals.

The fact that the occupied rhenium-based orbitals lie energetically below the sulfur-based orbitals can be attributed to the rigid geometry imposed by the C–C backbone of the bis(dithiolato) ligand. This effect has been extensively studied on complexes of type $[MoOS_4]^-$.[43] Changes in the energy of the sulfur-based out-of-plane orbitals with changes in the O–M–S–C dihedral angle were larger in comparison with those of the in-plane orbitals, for which the electron density is directed mainly along the metal–sulfur bond. Mixed level descriptions of bonding have been obtained by means of spin restricted calculations for $[MoO(edt)_2]^-$,[43] for which a MO diagram with ligand-based orbitals lying above the single occupied metal orbital has been obtained.

Electronic Spectra

The absorption spectra for $[ReO(1)]_2^{2-}$ simulated in the gas phase and in the presence of the solvent employing the TD-BLDZ DFT method are presented in Figure 7. Calculated spin allowed singlet-singlet electronic transitions in DMF are presented in Table 4. For the high energy part of the spectrum, only transition with oscillator strengths larger than 0.0020 are included. For all transitions, only orbital contributions larger than 10% were taken into account. No important shifts were detected on going from vacuum to a DMF solution.

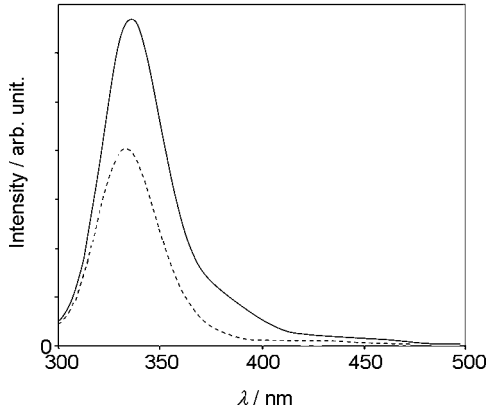

Figure 7. Electronic absorption spectra for $[ReO(1)]_2^{2-}$ calculated in vacuo (dashed line) and in DMF (solid line) employing the TD-BLDZ DFT methodology.

The lowest energy absorption band in vacuo (dashed line) calculated at 426 nm (see Table S10) can be described by the transitions HOMO–1 → LUMO+3 and HOMO → LUMO+2. Analysis of these MOs (Figure 6) shows that electron density are transferred from the sulfur donor atoms to the metal, which indicate that this transition has a very strong ligand-to-metal charge transfer (LMCT) character. In the same spectrum, the intense band at 333 nm is attributed to the transitions HOMO–1 → LUMO+4 and HOMO → LUMO+5, which can be attributed to a LMCT.

Table 4. Electronic transitions of $[ReO(\mathbf{1})]_2^{2-}$ calculated in DMF using the TD-BLDZ DFT method.

Most important orbital excitations[a]	λ [nm]	f	λ_{exp} [nm][b]
H-1 → L+2, H-1 → L+3, H → L+3	442.6	0.0017	
H-1 → L+3, H → L+2, H → L+3	442.6	0.0073	520 (sh)
H-9 → L+1, H-8 → L, H-4 → L, H-5 → L+1	436.4	0.0042	
H-9 → L+2, H-8 → L+3, H-5 → L+2, H-4 → L+3	428.8	0.0098	
H-3 → L, H-2 → L+1	380.0	0.0763	440 (sh)
H-2 → L+2, H-3 → L+3	370.7	0.0365	
H-4 → L, H-5 → L+1	367.6	0.0141	
H-6 → L+3, H-5 → L+2, H-4 → L+3	360.4	0.0177	
H-8 → L+1, H-7 → L, H-7 → L+1, H-6 → L, H-6 → L+1	347.5	0.0034	
H-8 → L, H-7 → L, H-7 → L+1, H-6 → L, H-6 → L+1	347.5	0.0042	
H-1 → L+4, H → L+5	334.9	0.8938	318
H-7 → L+1, H-6 → L	308.9	0.0038	
H-8 → L, H-7 → L, H-7 → L+1	306.8	0.0064	
H-1 → L+8, H-1 → L+9, H → L+8	306.8	0.0177	

[a] H = HOMO, L = LUMO. [b] sh = shoulder.

The simulated absorption spectrum in DMF (Figure 7, solid line) is in good agreement with the experimental one. An absorption band as a shoulder is calculated at 442 nm due to the transitions HOMO–1 → LUMO+3, HOMO → LUMO+2 and HOMO → LUMO+3, which appears about 80 nm blue-shifted relative to the experimental value of 520 nm. The features exhibited by the MOs involved (Figure 6) allow the assignment of this transition to be mainly a LMCT band. The same assignment can be made for the transition calculated at 380 nm, in which the electron density is transferred from the HOMO–3 and HOMO–2 MOs to the LUMO and LUMO+1 MOs. It should be emphasized that B3LYP in combination with LAN2DZ, taking the effects of the solvent into account, constitutes a unique method for the successful calculation of this absorption band.

In analogy to the results in the gas phase, an intense band in the high energy part of the calculated spectrum in DMF was found at 335 nm and assigned to the HOMO–1 → LUMO+4 and HOMO → LUMO+5 transitions. In this case, the electron density is transferred from sulfur-based MOs to rhenium-centered MOs. As can be seen in Figure 6, the LUMO+4 and LUMO+5 orbitals are delocalized among rhenium, the oxido and bis(dithiolato) ligands and thus delocalized ligand-to-metal-to-ligand charge transfer (LMLCT) leads to the observed bands.

Conclusions

In this work we have reported an experimental and theoretical study of a dinuclear double stranded oxido Re^V complex with a bis(benzene-*o*-dithiolato) ligand. The crystallographic results show a molecular structure in which two $\{ReO(bdt)_2\}$ units are bridged in a double-stranded fashion. The coordination geometry around the rhenium atom

is very similar to the coordination geometry previously reported for $[ReO(bdt)_2]^-$. The arrangement in a coplanar fashion of the planes defined by the four sulfur atoms at each rhenium center excludes the formation of a helical structure.

The Re^V complex exhibits a blue luminescence upon exciting its LMCT absorption band at 380–400 nm. The excited-state lifetime remained unaltered (about 10 ns) upon degassing the solution to remove O_2. This indicates that the emitting state is a singlet and can be represented by LMCT.

Calculations of structural and electronic properties, an analysis of the nature of the chemical bonds and of the excited state properties were performed by means of four DFT methodologies. The general trends of the crystallographical data were well reproduced using all four DFT methodologies. In describing Re–S bonds, PBE1PBE in combination with MIDI! and the Stuttgart energy consistent pseudopotentials, proved to be the best overall performer. The NBO method was able to detect the presence of three Re–O natural bonds, composed by one σ and two π bonds, all of them strongly polarized toward the non-metal. The d contributions dominate the hybridization at rhenium in the Re–O σ and π oxido bonds. For all sulfur donor atoms σ bonds were detected, which are strongly polarized toward the non-metal. The hybrid B3LYP functional in combination with the standard LANL2DZ basis set has proved to be the most appropriated to simulate the electronic spectra. The solvent effects have been successfully described, which enable a prediction of the low intensity absorption band experimentally observed at 440 nm.

Experimental Section

General: If not stated otherwise, manipulations were carried out under an atmosphere of dry argon by using standard Schlenk techniques. Methanol was freshly distilled from magnesium metal prior to use. ^1H and ^{13}C NMR spectra were obtained on Bruker AC200 NMR spectrometer (200 and 50 MHz, respectively) and are reported relative to TMS as internal standard. Mass spectrum (ESI) was obtained with a Micromass Quattro LC-Z spectrometer and IR spectra were recorded on a Bruker Vektor 22 spectrometer as a KBR pellet. UV/Vis absorption spectra were measured on a Varian Cary 50 spectrophotometer. $[ReOCl_3(PPh_3)_2]$[44] and 1,2-bis(2,3-dimercaptobenzamido)ethane (H_4-**1**)[21c] were prepared by employing reported methods.

$(Ph_4P)_2[ReO(1)]_2$: A solution of H_4-**1** (100 mg, 0.260 mmol) and Na_2CO_3 (110 mg, 1.04 mmol) in methanol (10 mL) was added dropwise to a suspension of $[ReOCl_3(PPh_3)_2]$ (217 mg, 0.260 mmol) in methanol (10 mL), giving rise to a green reaction mixture. While refluxing for 2 h, the green mixture changes the color to a brown solution. After filtration at room temperature in air, 98 mg (0.260 mmol) of PPh_4Cl was added to the filtrate with stirring. An orange precipitate (160 mg, 0.085 mmol, 65%) was separated by filtration and washed with diethyl ether (4 × 5 mL). The solid was dissolved in *N*,*N*-dimethylformamide. Vapor diffusion of diethyl ether into this solution yielded orange crystals of the *N*,*N*-dimethylformamide solvate $(Ph_4P)_2[ReO(\mathbf{1})_2]\cdot 2DMF$ which were suitable for X-ray diffraction studies. ^1H NMR for the solvent-free complex (200 MHz, [D_7]DMF): δ = 8.34 (m, 4 H, Ar-H), 7.87 (m, 40 H, P-Ph-H), 7.21 (m, 4 H, Ar-H), 7.04 (m, 4 H, Ar-H), 3.76 (m, 8 H, CH_2) ppm. ^{13}C NMR (50 MHz, [D_7]DMF): δ = 170.0 (CONH), 163.2, 162.7, 162.0, 138.0, 135.1, 131.6, 129.2, 124.8, 124.3, 122.1 (Ar-C), 40.2 (CH_2) ppm. IR (KBr): $\tilde{\nu}$ = 997 (Re≡O) cm^{-1}. MS (ESI, negative ions): m/z = 595 $[ReO(\mathbf{1})]_2^{2-}$.

Spectroscopic Measurements: Absorption spectra were measured on a Varian Cary 5000 double-beam UV/Vis/NIR spectrometer and baseline corrected. Steady-state emission spectra were recorded on a HORIBA Jobin–Yvon IBH FL-322 Fluorolog 3 spectrometer equipped with a 450 W xenon arc lamp, double-grating excitation and emission monochromators, and a Hamamatsu R928 photomultiplier tube or a TBX-4-X single-photon-counting detector. Emission and excitation spectra were corrected for source intensity (lamp and grating) and emission spectral response (detector and grating) by standard correction curves. Time-resolved measurements were performed using the time-correlated single-photon counting (TCSPC) option on the Fluorolog 3. A NanoLED (402 nm; FWHM < 750 ps) with repetition rates between 10 kHz and 1 MHz was used to excite the sample.

X-ray Diffraction Study: Diffraction data for $(PPh_4)_2[ReO(\mathbf{1})]_2\cdot 2DMF$ were collected with a Bruker AXS APEX CCD diffractometer equipped with a rotation anode at 153(2) K using graphite-monochromated Mo-K_α radiation (λ = 0.71073 Å). Diffraction data were collected over the full sphere ($17 \geq h \geq -17$, $13 \geq k \geq -13$, $31 \geq l \geq -31$, $50.6 \geq 2\theta \geq 2.8°$) and were corrected for absorption. The data reduction was performed with the Bruker SMART[45] program package. A structure solution was found with the SHELXS-97[46] package using the heavy-atom method and was refined with SHELXL-97[47] against $|F^2|$ using first isotropic and later anisotropic thermal parameters for all non-hydrogen atoms. Hydrogen atoms were added to the structure models on calculated positions. ORTEP-3 for Windows[48] was used for drawings.

Crystal Data for $(PPh_4)_2[ReO(1)]_2\cdot 2DMF$: $C_{86}H_{78}N_6O_8P_2Re_2S_8$, M = 2014.36, μ = 3.242 mm^{-1}, ρ = 1.626 g cm^{-3}, monoclinic, $P2_1/c$, Z = 2, a = 14.9424(12), b = 10.9108(9), c = 26.032(2) Å, β = 104.1890(10)°, V = 4114.6(6) $Å^3$, 32915 measured reflections, 7463 unique reflections (R_{int} = 0.0603), R = 0.0655, wR^2 = 0.1779 for 5122 contributing reflections [$I \geq 2\sigma(I)$], refinement against $|F^2|$ with anisotropic thermal parameters for all non-hydrogen atoms and hydrogen atoms on calculated positions. The asymmetric unit contains half a formula unit of $(PPh_4)_2[ReO(\mathbf{1})]_2\cdot 2DMF$.

CCDC-735417 contains the supplementary crystallographic data for this paper. These data can be obtained free of charge from The Cambridge Crystallographic Data Centre via www.ccdc.cam.ac.uk./data/request/cif.

Computational Details: All computational studies were performed at the density functional level of theory (DFT). The geometry was optimized in a closed-shell singlet (S = 1) state starting from the molecular structure determined by X-ray crystallography. It was reported[32] that in describing the Re–S bond, PBE1PBE in combination with the so-called STMIDI basis set (see below for details) has shown an excellent performance. For the study of the Re–O bond, however, B3LYP in combination with the standard LANL2DZ has proved to be an adequate method.[32] Therefore we decided to assess the four DFT methodologies arising from the combination of the aforementioned hybrid functionals and basis sets. The PBE1PBE is composed of the Perdew, Burke, Ernzerhof[49–51] exchange and a correlation functional with 25% HF exchange while B3LYP represent Becke's 1988 exchange functional[52] coupled with exact (i.e. Hartree–Fock) exchange as in Becke's publication,[53] and the Lee–Yang–Parr correlation potential.[54] For the metal atom, the core electrons (60) were treated through the pseu-

dopotential approximations (ECP) as included in the LANL2DZ[55] basis set. The valence electrons for non-metal atoms in STMIDI were treated with MIDI!,[56] those for the metal being described by a basis set (8s7p6d2f1g)/[6s5p3d2f1g].[57] The core electrons were replaced by Stuttgart effective core pseudopotentials.[57,58] These basis sets take relativistic effects into account, especially important when systems with heavy atoms are studied.[59] The nature of the stationary point was verified through a vibrational analysis (no imaginary frequencies). Time-dependent DFT (TD-DFT) method was employed to calculate 50 singlets transitions in the gas phase and in a DMF[60] solution, the latter being described by the conductor-like polarizable continuum model (C-PCM).[61,62] Electronic spectra were simulated by means of the GaussSum software[63] taking all calculated transitions into account. Natural bond orbital (NBO) calculations were performed with the NBO code[64–67] including in the program package Gaussian 03, Rev. D.02,[68] which has been used for all theoretical studies reported in this work.

Supporting Information (see also the footnote on the first page of this article): Details of the DFT calculations and the electronic transistions.

Acknowledgments

J. S. G. and R. Q. A. wish to thanks the Alexander von Humboldt Foundation for postdoctoral fellowships. We thank Dr. Alexander Hepp for measuring the NMR spectra and Dr. Heinrich Luftmann for measuring the mass spectra. Financial support by the Spanish Ministerio de Educación y Ciencia (MEC) is acknowledged by A. G.-M.

[1] U. Oetliker, C. Savoie, S. Stanislas, C. Reber, F. Connac, A. L. Beauchamp, F. Loiseau, M. Dartiguenave, *Chem. Commun.* **1998**, 657–658, and references therein.
[2] S. Dinga, M. G. B. Drew, R. Bhattacharyya, *Catal. Commun.* **2009**, *10*, 720–724.
[3] P. M. Reis, P. J. Costa, C. C. Romão, J. A. Fernándes, M. J. Calhorda, B. Royo, *Dalton Trans.* **2008**, 1727–1733.
[4] G. Du, P. E. Fanwick, M. M. Abu-Omar, *Inorg. Chim. Acta* **2008**, *361*, 3184–3192.
[5] A. Sachse, N. C. Mösch-Zanetti, G. Lyashenko, J. W. Wielandt, K. Most, J. Magull, F. Dall′Antonia, A. Pal, R. Herbst-Irmer, *Inorg. Chem.* **2007**, *46*, 7129–7135.
[6] B. D. Sherry, R. N. Loy, F. D. Toste, *J. Am. Chem. Soc.* **2004**, *126*, 4510–4511.
[7] M. M. Abu-Omar, S. I. Khan, *Inorg. Chem.* **1998**, *37*, 4979–4985.
[8] J. H. Espenson, *Coord. Chem. Rev.* **2005**, *249*, 329–341.
[9] J. H. Espenson, *Adv. Inorg. Chem.* **2003**, *54*, 158–202.
[10] C. Redshaw, X. Liu, S. Zhan, D. L. Hughes, H. Baillie-Johnson, M. R. J. Elsegood, S. H. Dale, *Eur. J. Inorg. Chem.* **2008**, 2698–2712.
[11] M. V. Cantorias, R. C. Howell, L. Todaro, J. E. Cyr, D. Berndorff, R. D. Rogers, L. C. Francesconi, *Inorg. Chem.* **2007**, *46*, 7326–7340.
[12] U. Choudhry, W. E. P. Greenland, W. A. Goddard, T. A. J. Maclennan, S. J. Teat, P. J. Blower, *Dalton Trans.* **2003**, 311–317.
[13] S. Tzanopoulou, I. C. Pirmettis, G. Patsis, C. Raptopoulou, A. Terzis, M. Papadopoulos, M. Pelecanou, *Inorg. Chem.* **2006**, *45*, 902–909.
[14] D. W. Lathi, J. H. Espenson, *J. Am. Chem. Soc.* **2001**, *123*, 6014–6024.
[15] X. Yang, M. B. Hall, *J. Am. Chem. Soc.* **2007**, *129*, 1560–1567.
[16] B. Noll, C. S. Hilger, P. Leibnitz, H. Spies, *Radiochim. Acta* **2004**, *92*, 271–276.
[17] A. Zablotskaya, I. Segal, S. Germane, I. Shestakova, E. Lukevics, T. Kniess, H. Spies, *Appl. Organomet. Chem.* **2002**, *16*, 550–555.
[18] F. E. Hahn, W. W. Seidel, *Angew. Chem. Int. Ed. Engl.* **1995**, *34*, 2700–2703.
[19] H. V. Huynh, W. W. Seidel, T. Lügger, R. Fröhlich, B. Wibbeling, F. E. Hahn, *Z. Naturforsch., Teil B* **2002**, *57*, 1401–1408.
[20] T. Kreickmann, F. E. Hahn, *Chem. Commun.* **2007**, 1111–1120.
[21] a) F. E. Hahn, B. Birkmann, T. Pape, *Dalton Trans.* **2008**, 2100–2102; b) T. Kreickmann, C. Diedrich, T. Pape, H. V. Huynh, S. Grimme, F. E. Hahn, *J. Am. Chem. Soc.* **2006**, *128*, 11808–11819; c) H. V. Hyunh, C. Schulze-Isfort, W. W. Seidel, T. Lügger, R. Fröhlich, O. Kataeva, F. E. Hahn, *Chem. Eur. J.* **2002**, *8*, 1327–1335; d) W. Seidel, F. E. Hahn, *J. Chem. Soc., Dalton Trans.* **1999**, 2237–2241.
[22] D. Sellmann, K. P. Peters, R. M. Molina, F. W. Heinemann, *Eur. J. Inorg. Chem.* **2003**, 903–907.
[23] W. W. Seidel, F. E. Hahn, *Bioinorg. Chem. Appl.* **2005**, *3*, 69–80.
[24] D. Morales-Morales, Y. Zheng, J. R. Dilworth, R. Redón, H. Torrens, *Inorg. Chim. Acta* **2001**, *314*, 37–41.
[25] B. Schmidt-Brücken, U. Abram, *Z. Anorg. Allg. Chem.* **2000**, *626*, 951–958.
[26] M. M. Lynam, J. C. Vites, *Coord. Chem. Rev.* **1997**, *162*, 319–344, and references therein.
[27] J. R. Dilworth, J. Hu, S.-X. Liu, J. A. K. Howard, D. C. Povey, *Inorg. Chim. Acta* **1994**, *223*, 63–69.
[28] W. Clegg, *Acta Crystallogr., Sect. C* **1988**, *44*, 172–174.
[29] A. W. Addison, T. N. Rao, J. Reedijk, J. van Rijn, G. C. Verschoor, *J. Chem. Soc., Dalton Trans.* **1984**, 1349–1356.
[30] R. Hübener, U. Abram, *Acta Crystallogr., Sect. C* **1993**, *49*, 1068–1070.
[31] J. M. Mayer, *Inorg. Chem.* **1988**, *27*, 3899–3903.
[32] J. S. Gancheff, P. A. Denis, E. F. Hahn, *J. Mol. Model.* **2009**, submitted for publication.
[33] B. Machura, J. Kusz, D. Tabak, R. Kruszynski, *Polyhedron* **2009**, *28*, 493–500.
[34] B. Machura, M. Jaworska, P. Lodowski, *THEOCHEM* **2006**, *766*, 1–8.
[35] P. Pyykkö, S. Riedel, M. Patzschke, *Chem. Eur. J.* **2005**, *11*, 3511–3520.
[36] A. Neuhaus, A. Veldkamp, G. Frenking, *Inorg. Chem.* **1994**, *33*, 5278–5286.
[37] O. Grtisenko, E. J. Baerends, *J. Chem. Phys.* **2004**, *121*, 655–660.
[38] A. Dreuw, M. J. Head-Gordon, *J. Am. Chem. Soc.* **2004**, *126*, 4007–4016.
[39] M. Turki, C. Daniel, S. Záliš, A. Vlček Jr., J. van Slageren, D. J. Stufkens, *J. Am. Chem. Soc.* **2001**, *123*, 11431–11440.
[40] J. S. Gancheff, P. A. Denis, E. F. Hahn, *Inorg. Chim. Acta*, submitted for publication.
[41] F. E. Inscore, R. McNaughton, B. L. Westcott, M. E. Helton, R. Jones, I. K. Dhawan, J. H. Enemark, K. L. Kirk, *Inorg. Chem.* **1999**, *38*, 1401–1410.
[42] M. D. Carducci, C. Brown, E. I. Solomon, J. H. Enemark, *J. Am. Chem. Soc.* **1994**, *116*, 11856–11868.
[43] J. McMaster, M. D. Carducci, Y. S. Yang, E. I. Solomon, J. H. Enemark, *Inorg. Chem.* **2001**, *40*, 687–702.
[44] N. P. Johnson, C. J. Lock, G. Wilkinson, *J. Chem. Soc.* **1964**, 1054–1066.
[45] *SMART*, Bruker AXS, **2000**.
[46] SHELXS-97: G. M. Sheldrick, *Acta Crystallogr., Sect. A* **1990**, *46*, 467–473.
[47] G. M. Sheldrick, *SHELXL-97*, University of Göttingen, Germany, **1997**.
[48] L. J. Farrugia, *ORTEP-3*, University of Glasgow, Scotland, **1999**.
[49] J. P. Perdew, K. Burke, M. Ernzerhof, *Phys. Rev. Lett.* **1996**, *77*, 3865–3868.
[50] C. Adamo, V. Barone, *J. Chem. Phys.* **1999**, *110*, 6158–6170.

[51] A. D. Becke, *J. Chem. Phys.* **1993**, *98*, 1372–1377.
[52] A. D. Becke, *Phys. Rev. A* **1988**, *38*, 3098–3100.
[53] A. D. Becke, *J. Chem. Phys.* **1993**, *98*, 5648–5652.
[54] C. Lee, W. Yang, R. G. Parr, *Phys. Rev. B* **1988**, *37*, 785–789.
[55] P. J. Hay, W. R. Wadt, *J. Chem. Phys.* **1985**, *82*, 299–310.
[56] R. E. Easton, D. J. Giesen, A. Welch, C. J. Cramer, D. G. Truhlar, *Theor. Chim. Acta* **1996**, *93*, 281–301.
[57] a) M. Dolg, U. Wedig, H. Stoll, H. Preuss, *J. Chem. Phys.* **1987**, *86*, 866–872; b) J. M. L. Martin, A. Sundermann, *J. Chem. Phys.* **2001**, *114*, 3408–3420; c) D. Andrae, U. Häussermann, M. Dolg, H. Stoll, H. Preuss, *Theor. Chim. Acta* **1990**, *77*, 123–141.
[58] A. Bergner, M. Dolg, W. Kuechle, H. Stoll, M. Preuss, *Mol. Phys.* **1993**, *80*, 1431–1441.
[59] P. Pyykkö, *The Effect of Relativity in Atoms, Molecules and The Solid State*, Plenum, New York, **1990**.
[60] E. S. Böes, P. R. Livotto, H. Stassen, *Chem. Phys.* **2006**, *331*, 142–158.
[61] V. Barone, M. Cossi, *J. Phys. Chem. A* **1998**, *102*, 1995–2001.
[62] M. Cossi, N. Rega, G. Scalmani, V. Barone, *J. Comput. Chem.* **2003**, *24*, 669–681.
[63] *GaussSum 0.8*, N. M. O'Boyle, J. G. Boss, Dublin City University, **2004**.
[64] J. P. Foster, F. Weinhold, *J. Am. Chem. Soc.* **1980**, *102*, 7211–7218.
[65] A. E. Reed, F. Weinhold, *J. Chem. Phys.* **1985**, *83*, 1736–1740.
[66] A. E. Reed, R. B. Weinstock, B. Weinhold, *J. Chem. Phys.* **1985**, *83*, 735–746.
[67] A. E. Reed, L. A. Curtis, F. Weinhold, *Chem. Rev.* **1988**, *88*, 899–926.
[68] M. J. Frisch, G. W. Trucks, H. B. Schlegel, G. E. Scuseria, M. A. Robb, J. R. Cheeseman, J. A. Montgomery Jr., T. Vreven, K. N. Kudin, J. C. Burant, J. M. Millam, S. S. Iyengar, J. Tomasi, V. Barone, B. Mennucci, M. Cossi, G. Scalmani, N. Rega, G. A. Petersson, H. Nakatsuji, M. Hada, M. Ehara, K. Toyota, R. Fukuda, J. Hasegawa, M. Ishida, T. Nakajima, Y. Honda, O. Kitao, H. Nakai, M. Klene, X. Li, J. E. Knox, H. P. Hratchian, J. B. Cross, V. Bakken, C. Adamo, J. Jaramillo, R. Gomperts, R. E. Stratmann, O. Yazyev, A. J. Austin, R. Cammi, C. Pomelli, J. W. Ochterski, P. Y. Ayala, K. Morokuma, G. A. Voth, P. Salvador, J. J. Dannenberg, V. G. Zakrzewski, S. Dapprich, A. D. Daniels, M. C. Strain, O. Farkas, D. K. Malick, A. D. Rabuck, K. Raghavachari, J. B. Foresman, J. V. Ortiz, Q. Cui, A. G. Baboul, S. Clifford, J. Cioslowski, B. B. Stefanov, G. Liu, A. Liashenko, P. Piskorz, I. Komaromi, R. L. Martin, D. J. Fox, T. Keith, M. A. Al-Laham, C. Y. Peng, A. Nanayakkara, M. Challacombe, P. M. W. Gill, B. Johnson, W. Chen, M. W. Wong, C. Gonzalez, J. A. Pople, *GAUSSIAN 03*, Rev. D.2, Gaussian, Inc., Wallingford CT, **2004**.

Received: June 4, 2009
Published Online: August 12, 2009

